Research Article | Vol. 30, No. 15 / 18 Jul 2022 / Optics Express 27730
Optics EXPRESS

Shape influence on the ultrafast plasmonic properties of gold nanoparticles

DOMANTAS PECKUS,[1,6] ASTA TAMULEVIČIENĖ,[1,2] KARINE MOUGIN,[3,4] ARNAUD SPANGENBERG,[3,4] LOIC VIDAL,[3,4] QUENTIN BAUERLIN,[3,4] MARC KELLER,[3,4] JOEL HENZIE,[5] LINAS PUODŽIUKYNAS,[2] TOMAS TAMULEVIČIUS,[1,2] AND SIGITAS TAMULEVIČIUS[1,2,7]

[1]*Institute of Materials Science of Kaunas University of Technology, K. Baršausko st. 59, LT-51423, Kaunas, Lithuania*
[2]*Department of Physics, Kaunas University of Technology, Studentų st. 50, LT-51368, Kaunas, Lithuania*
[3]*Institut de Science des Matériaux de Mulhouse IS2M UMR 7361, 15 rue Jean Starcky, F 68100 Mulhouse, France*
[4]*Université de Strasbourg, 4 Rue Blaise Pascal, CS 90032, F-67081 Strasbourg, France*
[5]*International Center for Materials Nanoarchitectonics (WPI-MANA), National Institute for Materials Science (NIMS), Tsukuba, 305-0044, Japan*
[6]*domantas.peckus@ktu.lt*
[7]*sigitas.tamulevicius@ktu.lt*

Abstract: The aim of shape-controlled colloidal synthesis of gold (Au) is to produce Au nanoparticles (NPs) with fine control of shapes, sizes, and dispersities. We show how transient absorption spectroscopy (TAS) can be used to rapidly and accurately quantify the vast ensemble of shapes of Au NPs in solution within minutes, including the synthesized nanorods, decahedra, and nanospheres. Colloidal solutions containing Au NPs were measured in TAS and their localized surface plasmon resonance (LSPR) modes were classified according to the shape, wavelength and number of peaks. Then their excited-state relaxation dynamics were used to ascertain their electron-phonon (*e-ph*) coupling time constant and frequency of optomechanical modes. TAS can quickly show that an Au nanosphere sample contains a tiny fraction of Au nanorods, whereas steady-state absorbance is totally blind to the presence of nanorods. Additionally, the TAS experiments indicate that the characteristic *e-ph* coupling time constants in Au nanorods depend on the NPs dimensions at high excitation intensity (> 6 μJ/cm^2) which can help identify if there are any elongated Au NPs in Au spheres samples. Finally, optomechanical oscillations formed by NPs breathing modes were observed, providing information related to the average size and monodispersity of Au nanospheres and nanorods.

1. Introduction

Recently, plasmonic metal nanoparticles (NPs) due to their localized surface plasmon resonance (LSPR) properties have shown great promise in various electro-optical applications, including solar cells [1], photocatalysis [2], nonlinear optics [3], medicine [4], bioimaging [5], etc. The LSPR is a collective excitation of free electrons that can focus and manipulate light to deeply subwavelength scales. The LSPR wavelength and bandwidth depend on the dielectric function of the metal, in addition to the size, shape, and internal structure of the NPs [6]. Due to well-characterized unique electronic and physical properties and well-established synthesis methods, gold NPs are a versatile platform for fundamental plasmonics research, point-of-care medical diagnostic testing, and some industrial products [7]. For example, shaped Au NPs with sharp tips and vertices have been widely used as high-sensitivity LSPR-based sensors [8]. Recent biomedical applications of Au NPs with an emphasis on cancer diagnostics and therapeutics

#463961 https://doi.org/10.1364/OE.463961
Journal © 2022 Received 18 May 2022; revised 16 Jun 2022; accepted 16 Jun 2022; published 14 Jul 2022

Optics EXPRESS

have been reported in [9], where the LSPR enhanced optical absorption of Au nanospheres and nanorods was used for plasmonic photothermal therapy of cancer [10]. The potential use of gold NPs as imaging contrast agents for clinical intracoronary frequency-domain optical coherence tomography was explored in [11].

Further advances in the field require more robust methods to rapidly determine shape polydispersity in different NP synthesis batches. Scanning electron microscopy (SEM) and high resolution transmission electron microscopy (HRTEM) are frequently used for shape analysis. But neither SEM or HRTEM are ensemble measurements, meaning particles must be measured individually, so the spatial resolution of the method is very important and information on the 3D shape is difficult to extract from 2D images [12–16]. Thus hundreds or thousands of particles must be measured in order to represent the statistical variation of an ensemble solution of nanoparticles hence real-time monitoring of the ensemble is not possible. Techniques such as in-situ TEM can measure the evolution of shape of a few nanoparticles but the dynamics of NP growth are influenced by the presence of an electron beam [17]. Otherwise researchers can use X-ray methods, but typical colloidal solutions that are relatively dilute often require ultrabright synchrotron sources to interrogate size, crystallinity and shape [18]. Optical methods such as steady-state UV-absorption spectroscopy (UV-Vis) are ubiquitous in most labs and are a good method to rapidly estimate the dominant size/shape of ensembles of nanoparticles even in dilute solutions because of the large absorbance cross-sections generated by LSPRs [15,16,19,20]. UV-Vis data can be compared with electrodynamics models to estimate the average size of spheres with an accuracy of ~6% versus values estimated with HRTEM [15]. However, UV-Vis is often blind to other shapes with small concentrations even when those particles have vastly different LSPR resonance wavelengths. Transient absorbance spectroscopy (TAS) a more complex and expensive technique than UV-Vis but is an analytical tool that is about as common as HRTEM in most large institutions. And like UV-Vis methods, TAS can measure dilute or concentrated solutions used in colloidal synthesis by modifying the path length of the liquid cell. However, TAS offers insight into the internal dynamical processes of the ensemble of NPs, which are controlled in part by their size and shape.

Here we propose using TAS as a fast optical method to support NP synthesis because different Au NP shapes often have distinct absorbance properties and LSPR relaxation time constants at ultrashort time scale under high excitation intensities. TAS can, in principle, detect NPs with small concentrations that would be otherwise undetectable in UV-Vis, providing relatively fast real-time feedback on shape analysis and control in synthetic experiments. Unlike the steady-state absorption, TAS enables time-resolved characterization of the relaxation processes in the NPs. In addition, TAS offers a multiparameter plasmonic NPs analysis platform capable of evaluating NP size and shape based on the ultrafast time evolution of internal dynamical processes via the LSPR [21].

The LSPR relaxation dynamics start with the absorption of a photon and then dephasing of the plasmon (~10 fs), electron−electron scattering (~100 fs), electron−phonon coupling (~1 ps), and finally ends with mechanical oscillations and coupling to the environment (phonon-phonon scattering) (~1 ns) (Fig. 1 a) [6,22,23]. The characteristic decay constants can be used when selecting plasmonic metal NPs for their targeted applications. For example, NPs with long (> 1 ps) electron−phonon (*e-ph*) coupling time constants are advantageous in photocatalysis and solar cells. In comparison, NPs with a short *e-ph* coupling time (< 1 ps) are useful in photothermal applications such as cancer therapy [4]. It is also known that *e-ph* coupling time could give information about the crystal structure of analyzed NPs (Fig. 1 b) [24]. It has long been suggested that *e-ph* coupling time does not depend on the size and shape of Au NPs, particularly at low excitation intensities [25,26]. However, recent experiments on high-purity monocrystalline Au NP samples showed that the *e-ph* coupling strength decreases as particle diameter increases [27]. Moreover, high excitation intensities can also arouse size dependence in Au NP *e-ph* coupling

Optics EXPRESS

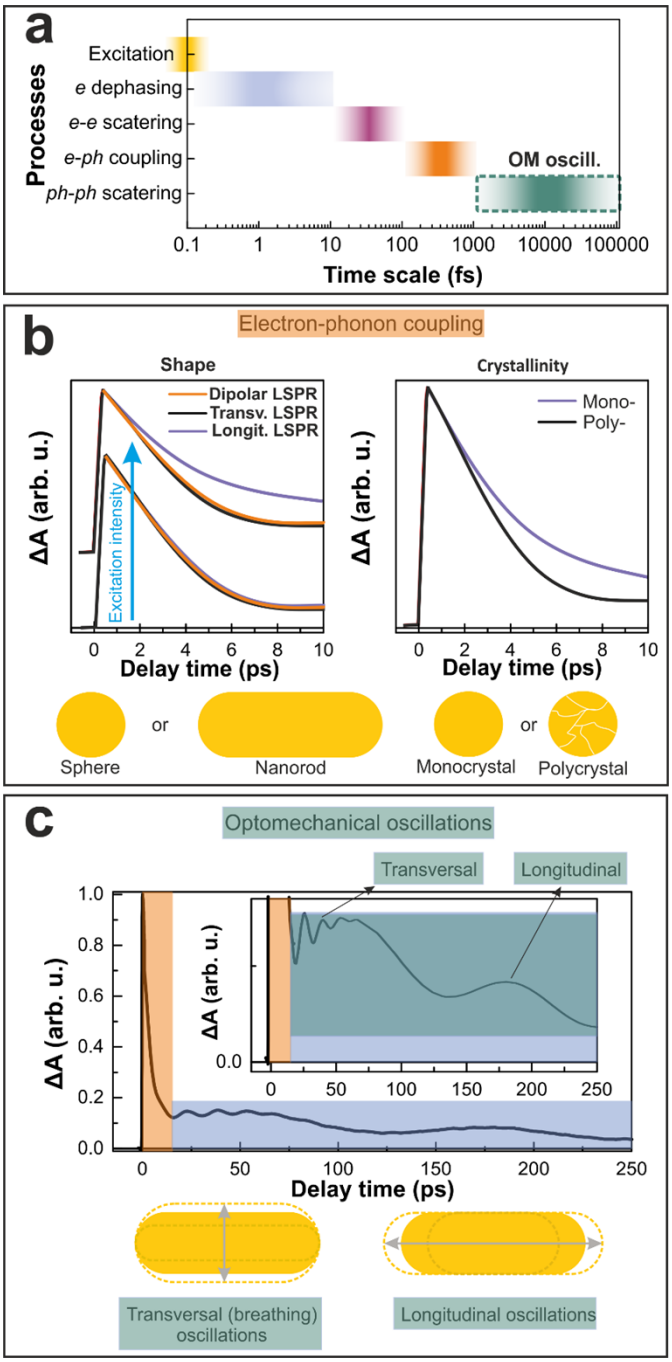

Fig. 1. The typical sequence of decay processes in gold nanoparticles. (**a**) Evolution of characteristic ultrafast processes in LSPR relaxation dynamics. Relationship between NP size, shape, and twinning defects of Au nanoparticles on their electron-phonon coupling (**b**) and optomechanical oscillations (**c**).

Optics EXPRESS

times, even in polycrystalline nanoparticles that usually do not show *e-ph* coupling dependence on size (Fig. 1 a, b) [28]. Thus *e-ph* coupling times provide another piece of data to analyze Au NP size and crystallinity (Fig. 1 a, b).

Longer time scales in TAS, ranging from picoseconds to nanoseconds provide additional shape/size information in the form of optomechanical oscillations [6]. When NP solutions are sufficiently monodisperse and when NPs are excited with laser sources faster than the period of thermal expansion/contraction, they can vibrate coherently (Fig. 1 a, c). Analysis of the optomechanical oscillation modes is interesting in the context of assessing nanoparticle shape with TAS because they provide information on NP size, temperature, crystal structure, and environment [6,29–32]. TAS has become a common technique for examining the ultrafast electronic dynamics of nanosized systems because tiny changes in absorbance indicate the flow of energy over short time scales [6,22]. It is known that the size and shape of the nanoparticles do not significantly influence the *e-ph* coupling relaxation time, [6] but these factors significantly influence the TAS spectra [33,34], including any optomechanical oscillations (Fig. 1 c) [29,30,33,35–37]. Besides the overview TAS spectra analysis, the in-depth characterization of mentioned parameters like TAS spectra, TAS signal relaxation time constants, and optomechanical oscillation could provide detailed information about the size, shape, and crystal structure of NPs from a single measurement in the future. In the present study, we have examined how the shape of gold NPs influences their spectral-dependent LSPR relaxation and its dynamics. Colloidal solutions containing Au nanorods, high-quality Au nanospheres, Au decahedra, and Au nanospheres with traces of nanorods were excited. Their LSPRs related to dipole or transversal and longitudinal modes were studied in HRTEM, UV-Vis, and TAS. The primary analysis revealed that TAS was able to highlight some NP shape-related differences that were hindered in UV-Vis spectra and were obvious only from the detailed electron micrograph statistical analysis. Moreover, an in-depth analysis of the TAS spectra time evolution confirmed that this method could be applied for the Au NPs indirect shape characterization through the differences in electron-phonon decay rate constants and optomechanical oscillation parameters.

2. Materials and methods

2.1. Nanomaterial synthesis

All chemicals were obtained from commercial suppliers and used without further purification. Hexadecyltrimethylammonium bromide (CTAB, ≥ 99.0%), sodium oleate (NaOL, ≥ 99.0%), hydrogen tetrachloroaurate trihydrate ($HAuCl_4 \cdot 3H_2O$), L-ascorbic acid (99%), silver nitrate ($AgNO_3$, > 99%), sodium borohydride ($NaBH_4$, ≥ 99%), hydrochloric acid (HCl, 37 wt.% in water) were purchased from Sigma Aldrich.

Synthesis of Au nanospheres. 250 mL of 0.01 wt.% of $HAuCl_4$ in an aqueous solution was prepared and then heated at 80°C. A 1% by weight aqueous sodium citrate solution has been prepared, and 5 mL of this solution has been added to the first solution under rapid stirring (1200 rpm). After 30 min of stirring, the final nanocolloidal gold particles solution was cooled down and was ready to use.

Synthesis of Au nanorods. This synthesis involved two distinct solutions: the seed and growth solutions. Preparation of the seed solution. 500 µL of 0.5 mM tetrachloroauric acid ($HAuCl_4$) solution and 500 µL of 0.2 M CTAB solution were mixed. 60 µL of a 0.01 M $NaBH_4$ solution (fresh) has been injected into 40 µL of distilled water. Then, the latter solution was added to the Au(III)-CTAB mixture under vigorous stirring (1200 rpm). After shaking for two minutes, the solution turned from yellow to brown-yellow, and the solution was left to stand for 30 minutes at room temperature before use.

Preparation of the growth solution. 125 mL of distilled water in a 500 mL Erlenmeyer flask was heated to 50°C. When the temperature reached 50°C, 3.5 g of CTAB and 0.617 g of sodium oleate (NaOL) were added and allowed to dissolve. The solution was cooled down to 30°C then

Optics EXPRESS

9 mL of freshly prepared $AgNO_3$ (4 mM) solution was added under vigorous stirring (1200 rpm). The stirring was then paused for 15 min, then 125 mL of $HAuCl_4$ solution (1 mM) was added under strong stirring (1200 rpm). The stirring was reduced to 700 rpm and over 90 minutes the solution became colorless. Lastly, 1.05 mL of 12.1 M HCl solution (37 wt.% in water) was added under strong stirring (1200 rpm). Then stirring was reduced to 400 rpm for 15 min, and 625 µL of a 0.064 M ascorbic acid (AA) solution (fresh) was injected. The solution was mixed vigorously (1200 rpm) and stirred for 30 s, and then a 400 µL of seed solution was added and mixed for an additional 30 s. Finally, the solution was left to stand unstirred at 30°C for 12 h.

Synthesis of decahedra Au nanoparticle seeds. A silicone oil bath was preheated to 90°C. 10 mL of DI water was put into a 20 mL vial and put on ice. A 60 mL vial was taken, 40 mL added then mixed at ~600 rpm. 5 mL of hexadecyltrimethylammonium chloride (CTAC) solution (0.5 M), 1.25 mL $HAuCl_4$ solution (0.01 M), and 2.5 mL of citric acid (0.1 M) were added and mixed for a few minutes. 23.6 mg of $NaBH_4$ was put into the 20 mL vial previously on ice and dissolved by vortexing. 1.25 mL of the $NaBH_4$ solution was added to the 60 mL vial and mixed for 2 minutes. The 60 mL vial was put into the oil bath and heated for 2 hours.

Synthesis of decahedra Au nanoparticles: 40 mL of 0.15 M CTAC was added to a 60 mL vial and stirred at 600 rpm. 2 mL $HAuCl_4$ solution (0.01 M), 1.2 mL $AgNO_3$ (0.01 M), 0.3 mL HCl (1 M), 0.32 mL Ascorbic acid (0.1 M) were added in sequence and stirred for 1 minute. Then 2 mL of the seed solution above was added and heated at 30°C for 12 hours with no stirring.

Synthesis of high-quality monodisperse Au nanospheres. Monodispersed Au nanospheres were produced in two-step synthesis according to [38]. In brief, at first seed solution was prepared by heating 150 mL of 2.2 mM sodium citrate solution to boiling, then 1 mL of $HAuCl_4$ (25 mM) was injected under vigorous stirring. The solution was kept at 100°C temperature for 10 minutes while the color of the solution changed from yellow to soft pink. Later this seed solution was used for the growth of nanoparticles. The temperature of the seed solution was reduced to 90°C, and 1 mL of $HAuCl_4$ (25 mM) was injected. Then the solution was left for 30 minutes at the same temperature. The procedure was repeated twice. Afterward, the solution was cooled in an ice bath to quench the reaction. These nanospheres demonstrated the best monodispersity of the investigated samples; therefore in this manuscript we call them high-quality Au nanospheres.

2.2. Characterization methods

Nanoparticle size distributions were evaluated from the transmission electron microscope micrographs: Au decahedra nanoparticles were investigated employing 2100F (JEOL) operating at 200 kV, while Au nanorods and nanospheres with traces of nanorods were investigated with ARM—200F (JEOL) operating at 200 kV. High-quality monodispersed Au nanospheres were acquired using TEM Tecnai G2 F20 X-TWIN (FEI, Netherlands) with a Schottky-type field emission electron source operated at 200 kV. TEM micrographs of gold NPs were analyzed with ImageJ 1.53e software.

Steady-state absorption spectra were recorded with UV-VIS-NIR steady-state absorption spectrometer AvaSpec-2048 and AvaLight-DHc light dual lamp deuterium and halogen source (Avantes, NED) covering 200-1100 nm spectral range with 1.4 nm spectral resolution.

Ultrafast relaxation processes in Au NPs (nanorods, high-quality nanospheres, decahedra, and nanospheres with traces of nanorods) were investigated employing a transient absorption spectrometer HARPIA (Light Conversion, LT). The system was excited using an ultrafast 290 fs pulse length and 1030 nm wavelength Yb:KGW laser Pharos (Light Conversion, LT) with a regenerative amplifier at a 66.7 kHz repetition rate. The pump beam wavelength based on the LSPR absorption maxima of the investigated NPs was tuned to 350, 470, 550, 720 nm with a collinear optical parametric generator Orpheus and harmonic generator Lyra (Light Conversion, LT). Then the samples were probed with a white light supercontinuum generated using a 2 mm thickness sapphire plate excited with a fundamental laser wavelength (1030 nm). The spectral

Optics EXPRESS

range of the supercontinuum probe as well as the detection range of the TAS dynamics spanned wavelengths from 476 to 782 nm. The excitation beam was focused on the 1 mm optical path length quartz cuvette (Hellma Analytics) to an approximately 700 µm diameter spot, and it was overlaid with the supercontinuum probe that was approximately 500 µm in diameter. The volume of the Au nanoparticle sample in water analyzed by TAS was approximately 2×10^{-7} mm^3.

3. Results and discussion

During our research, we have analyzed Au nanorods, high-quality nanospheres, decahedra [39], and nanospheres with traces of nanorods. We have investigated how the shape of nanoparticles influences the steady-state absorption and transient absorption spectra, while the TEM images were used to confirm the shape and monodispersity of Au NPs (Fig. 2 a, e, i, m). The average linear dimensions of the analyzed NPs are summarized in Table 1. The analyzed micrographs and their respective size distribution histograms are presented in the supplementary materials (Fig. S1-S8). Nanorods, high-quality nanospheres, and decahedra were highly monodisperse in shape, while nanospheres had up to 25% of ellipsoids.

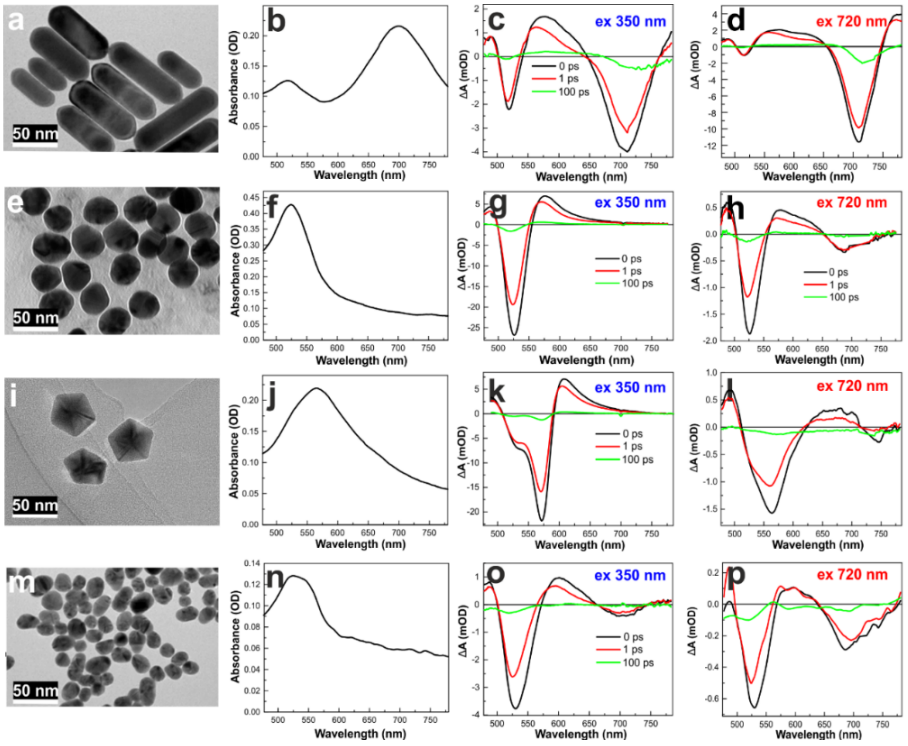

Fig. 2. TEM micrographs, UV-VIS absorption spectra (extension in Fig. S7), and TAS spectra measured under excitation (ex) at 350 and 720 nm (indicated in the legends) of Au nanorods (**a**, **b**, **c, d**), Au high-quality spheres (**e**, **f, g, h**), Au high-quality decahedra (**i, j, k, l**) and Au nanospheres with traces of nanorods (**m, n, o, p**). Ex 350 nm, 25.6 µJ/cm^2 and 720 nm, 80 µJ/cm^2. Visualized explanation of Au nanoparticle shape influence on TAS spectra is displayed in Fig. S10.

3.1. Transient absorption spectra dependencies on the shape of nanoparticles

As expected, the steady-state absorption spectra of the Au nanostructures had an LSPR band that depends on the size and shape of the Au NPs. Spherical NPs have a single peak related to

Optics EXPRESS

Table 1. The average linear dimensions of the analyzed nanoparticles.r with different length under the backward pumping regime.[a]

Type of NPs	Description	No. of NPs investigated (count)	Mean diameter / width / edge length (nm)	Average length (nm)	Aspect ratio (r.u.) / ellipsoid fraction (%)
Nanorods	**-**	71	28 ± 3 (10.7%)*	73 ± 12 (16.4%)	2.6
Nanospheres	**High quality**	78	33 ± 4 (12.1%)	-	-
Decahedra	**-**	20	27 ± 4 (15%)	-	-
Nanospheres with nanorods	**Nanospheres**	377	20 ± 5 (25%)	-	~25%
	Nanorods in nanospheres	16	18 ± 3 (17%)	30 ± 3 (10%)	1.7

[a]The error stands for one standard deviation. Value in parenthesis in percent represents polydispersity of the NP sizes.
[a]*Parenthesis shows relative deviation.

the dipole resonance, while nanorods demonstrated transversal mode and longitudinal mode LSPR peaks. The absorption peak in the UV-Vis spectra of nanorods at shorter wavelengths (515 nm) can be attributed to the absorption due to transversal dipole LSPR mode, while the peak at the longer wavelength (700 nm) matches the longitudinal dipole LSPR mode (Fig. 2 b) [40]. Measured absorption spectra match the modeling data described in Ref. [41]. The two peaks seen in the UV-Vis spectra (515 and 700 nm) can be directly related to the two negative peaks in the TAS spectra (520 and 710 nm) that are visible despite the chosen excitation at 350 or 720 nm (Fig. 2 a, b, c, d). Negative LSPR peaks in TAS spectra represent bleaching of the ground state [42].

One absorption peak in the visible spectral range at 525 nm was observed for high-quality Au nanospheres (Fig. 2 f). High-quality Au nanospheres (Fig. 2 e) have one negative TAS signal peak at 525 nm but no negative TAS signal at 700 nm under excitation of 350 nm (Fig. 2 g). While under excitation at 720 nm there is a weak TAS signal at 700 nm probably because some Au spheres are a bit elongated (Fig. S3), or it can be attributed to interband and intraband transitions in Au NPs [43].

The single LSPR peak at 572 nm recorded in the UV-Vis spectra for decahedra (Fig. 2 j) is also present as a negative TAS peak at 572 nm with an apparent shoulder at 530 nm under excitation at 350 nm (Fig. 2 i, j, k, l). Therefore, the shoulder peak can be attributed to the shape of NPs (Fig. 2 k) and can be used to distinguish the shapes of nanospheres and decahedra (Fig. 2 g, k, o). The difference in TAS spectra under excitation at 350 and 720 nm (Fig. 2 k, l) can be explained similarly for high-quality Au nanospheres (Fig. 2 g, h).

In steady-state absorbance, Au nanospheres with traces of nanorods exhibit a single peak at 525 nm, and yet have two peaks in the TAS measurement (530 and 700 nm) under excitation at 350 and 720 nm (Fig. 2 m, n, o, p). In principle, monodisperse Au nanospheres with an average size of 20 nm should not produce such a TAS signal at 700 nm, thus it is likely caused by different shape NPs. Even though steady-state absorption spectra of the nanospheres with traces of nanorods display only a single absorption peak, similarly to high-quality spheres (Fig. 2 f), decahedra (Fig. 2 j), or reported for similar size spheres elsewhere [44], the TEM micrographs confirm the presence of a small fraction of elongated NPs and nanorods in our samples (Fig. 2 m, S7, Table 1). Therefore, we attribute this negative TAS signal (700 nm) to the presence of nanorods and their related longitudinal LSPR resonance. Similarly, to the discussed case of the pure nanorod sample (Fig. 2 c, d). The traces of nanorods with an aspect ratio of 1.7 should produce a negative peak of TAS signal below 700 nm, but because of the positive TAS signal of spheres in spectral area of 600-650 nm most likely negative TAS signal is shifted to 700 nm.

Optics EXPRESS

The excitation of longitudinal dipole LSPR in Au nanorods is much more efficient than dipole LSPR Au nanospheres because it has a much larger absorbance cross-section; that is why we have received such an intense TAS signal that can be attributed to Au nanorods. It is most likely that two-photon absorption of the pump under excitation at 720 nm do not give any significant impact to the TAS signal because in that case TAS spectra under excitation at 350 nm and 720 nm (two-photon pump 360 nm) should look qualitatively similar and it is not the case as seen from Fig. 2 g, h; k, l; o, p [45].

Interestingly, even minor differences in the NP form of spheres *vs.* decahedra or a small number of nanorods in a sphere-dominated colloid can influence the TAS spectra, and the TAS method seems to be much more sensitive in comparison with the steady-state optical absorption (Fig. S10). The optical absorption spectra of high-quality Au nanospheres, decahedra, and nanospheres with traces of nanorods seem quite similar (Fig. 2 f, j, n), while TAS spectra clearly indicate the existence of nanorods in the nanospheres sample (Fig. 2 o, p). This observation can be useful in the future for the fast shape evaluation and analysis of plasmonic nanospheres or other sphere-like symmetrical structures (polyhedrons) from representative TAS spectra without deeper time-evolution analysis. It is worth noting that typical time resolved TAS measurement analyzed in this manuscript lasted for 20 min on average, and higher repetition systems using oscillators for excitation could speed up even further. While measurement of single TAS spectra at a specific delay time, *e.g.*, at 0 ps as depicted in Fig. 2 c, d, g, h, k, l, o, p could take up to 10 s therefore measurement of TAS spectra at a specific delay time can be as fast as steady-state optical absorption measurement but give more accurate information providing relatively fast real-time feedback on shape.

In this section, we have displayed that TAS spectra can be useful for real-time monitoring of the shapes of NPs and useful data can be received within a few seconds of measurements. Having full-time scale TAS measurement data, additional degrees of freedom can be evaluated like different decay constants and evolution of spectral changes in time. For in-depth TAS studies, including (i) excitation wavelength and (ii) intensity dependence, we have picked Au nanorods because they exhibit more complex LSPR features in comparison to spheres or decahedra NPs. One of these features is that Au nanorods have transversal and longitudinal dipole LSPR modes, while Au spheres and decahedra have single dipole LSPR only. Additionally, as we have seen previously, TAS is very sensitive to longitudinal LSPR (Fig. 2 o, p); therefore, more profound analysis of this phenomenon is necessary. The results of these findings are provided in the next section (section 3.2.). Moreover, laser-induced optomechanical oscillations of nanorods and nanospheres were investigated and discussed in section 3.3.

3.2. *Excited-state relaxation dynamics dependence on the excitation wavelength, the shape of nanoparticles, and excitation intensity*

Dynamic optical properties of Au nanorods were measured by TAS under four excitation wavelengths at 350, 470, 550, and 720 nm (Fig. 3, Fig. S11) applying different delay times (0–200 ps). One can see that the TAS spectra under excitation at 350, 470, and 550 nm seem quite similar. While the TAS spectra of Au nanorods excited at 720 nm are different. Here the second negative TAS band (650-750 nm) has a relatively much larger amplitude in comparison to the first one (500-540 nm) (Fig. 3 d). That is likely to be related to the two LSPR resonances present in the elongated nanoparticles because the first three wavelengths used for excitation overlay with the transversal LSPR while the longest one is next to the longitudinal resonance (Fig. 2 b).

As already discussed, Au nanorods have transversal and longitudinal LSPR modes. In the case of our study, it seems that under excitation at 350, 470, and 550 nm we have excited transversal mode while under excitation at 720 nm – longitudinal mode in the nanorods sample. The sample of Au nanospheres with traces of Au nanorods shows similar tendencies. The second negative

Optics EXPRESS

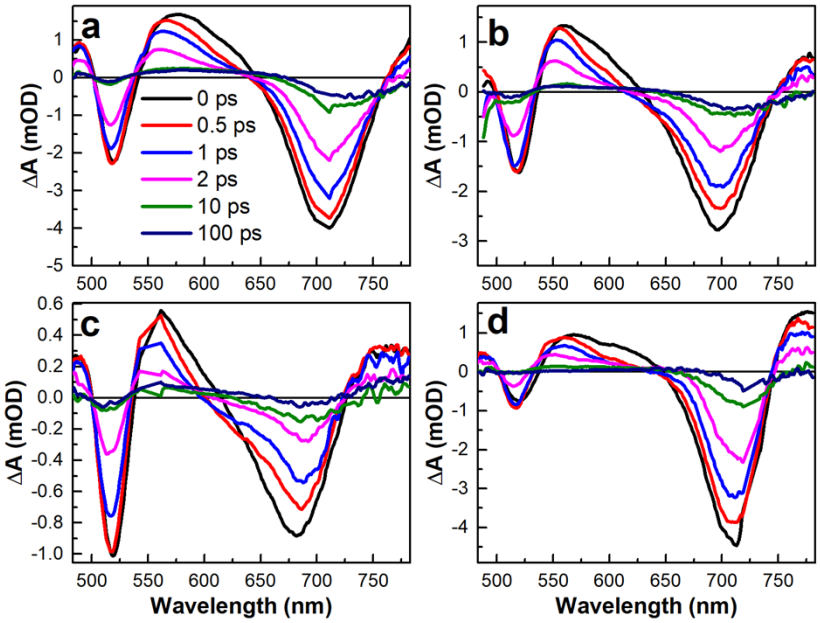

Fig. 3. TAS spectra evolution in time (from 0 to 100 ps as indicated in the legend) of Au nanorods in water obtained using different excitation wavelengths: (**a**) 350 nm, 25.6 μJ/cm^2; (**b**) 470 nm, 16 μJ/cm^2; (**c**) 550 nm, 11.2 μJ/cm^2; (**d**) 720 nm, 12 μJ/cm^2.

TAS signal (650-750 nm) peak that corresponds to longitudinal LSPR dominates TAS signal even under excitation of the transversal LSPR absorption band (350 nm) and its intensity becomes much larger under excitation at 720 nm (Fig. 3). Very intense longitudinal LSPR peak in TAS signal can explain why we can distinguish Au nanorods in Au nanospheres with TAS while we could not observe it in UV-Vis.

The characteristic decay constants of the four investigated Au nanostructure types of the same scale linear dimensions were also analyzed under unified excitation conditions. The decay constants were extracted from the analysis of the TAS evolution in time, i.e., fitting the traces using two exponent decay described by eq. (S1), we have determined how the excitation wavelength influences the excited state relaxation dynamics. The characteristic *e-ph* coupling (τ_1) and *ph-ph* scattering (τ_2) times (Fig. 1) were extracted from the experimental traces. The TAS spectra and traces of Au nanorods obtained under different excitation wavelengths and intensities are depicted in Fig. 3, and supplemental Fig. S11-13. The characteristic time constants and amplitudes representing one or two-component decay process were measured [46] to explain the differences in the four types of nanoparticle solutions are tabulated for nanorods in Tables S1-S2, for high-quality spheres in Fig. S14 and Table S3, for decahedra in Fig. S15 and Table S4, for nanosphere solutions with traces of nanorods in Fig. S16 and Table S5.

All measured samples have shown quite large *e-ph* coupling time constants (above ~1.5 ps) (Fig. 4 a, Table S1-S5) that can be useful for photocatalysis [2] or solar cells [3]. Interestingly, Au nanoparticles of different shapes have demonstrated different *e-ph* coupling time constants (Fig. 4 a). It is generally accepted that the *e-ph* coupling time constant does not depend on the shape of gold nanoparticles [26] but depends on crystalline structure or its defectiveness [47]. It should be noted that the decay time constants were determined under unified excitation conditions as all investigated samples were excited at 350 nm and 720 nm the wavelengths. We assume that *e-ph* coupling time constants determined under excitation at 350 nm might be more reliable because most samples except Au nanorods have a bigger optical density in this spectral

Optics EXPRESS

region (Fig. S9). *e-ph* coupling time constants were compared at characteristic traces at 515-530 nm that can be attributed to either transversal dipole LSPR (T-LSPR) resonance for elongated nanoparticles or to dipole LSPR (D-LSPR) for spherical nanoparticles (Fig. 4 a). The smallest *e-ph* coupling time constant using 350 nm excitation was obtained for nanospheres with traces of nanorods while the largest was for decahedra (Fig. 4 a) ranging from 1.8 to 2.8 ps. The smallest *e-ph* coupling time constant of high-quality Au nanospheres and Au nanospheres with traces of nanorods indicates that these nanoparticles are polycrystalline and their grain sizes are smaller than of other investigated nanostructures. The decahedra nanoparticles demonstrating the largest *e-ph* coupling are also multi-twinned [24,47,48] and therefore also polycrystalline but their grain sizes could be bigger than of our analyzed spheres.

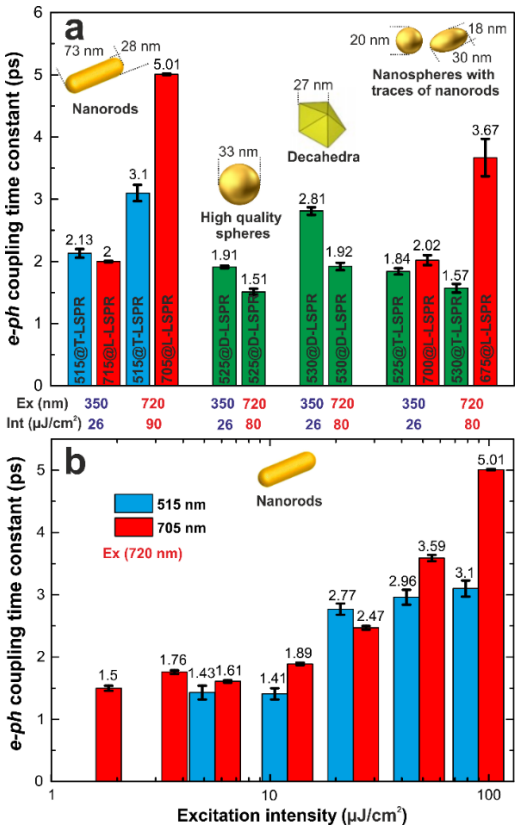

Fig. 4. *e-ph* coupling time constants of Au nanorods, Au high-quality nanospheres, Au decahedra, Au nanospheres with traces of nanorods exited at 350 and 720 nm at intensities indicated at the bottom and traces indicated on the bars (**a**). Au nanorod *e-ph* coupling time constant dependence on the excitation intensity with 720 nm wavelength at traces of 515 nm and 705 nm (**b**).

The *e-ph* data for both the transverse and longitudinal LSPR of the Au nanorods was included in Fig. 4 a. The longitudinal LSPR resonance excited with 720 nm decays longest and is in line with the observation of the Au sphere sample with traces of nanorods (Fig. 4 a). While the *e-ph* decay time constants obtained at 350 nm excitation are very close to the constants obtained for other shapes.

Keeping in mind rich information in the case of Au nanorods and their noticeable differences in the decay constants, they were used for the further excitation wavelength and intensity studies.

Optics EXPRESS

Analyzing the influence of the excitation intensity on the T-LSPR and L-LSPR relaxation dynamics, we found quite large value differences of the decay time constants ranging from 1.5 to 5 ps. On the other hand, it is worth recalling that the excitation intensity can influence the *e-ph* coupling decay time [49]. To verify this dependence, we have excited Au nanorods at 720 nm with various excitation intensities that varied from 1.6 to 89.6 μJ/cm^2. The measured TAS spectra and corresponding traces are demonstrated in Fig. S12 and Fig. S13, respectively. Transversal and longitudinal dipole LSPR modes related to TAS traces at 515 nm and 705 nm seen in Fig. S12 and S13 were selected for deeper excited state relaxation analysis. The fitting parameters are summarized in Table S2 and *e-ph* dependence on excitation intensity is depicted in Fig. 4 b.

Under low excitation intensity of 5.6 μJ/cm^2 the *e-ph* coupling time constant for TAS traces at 515 and 705 nm are quite similar and equals to ~1.5 ps, similarly like in Ref. [26]. The spectral dependence emerges with an increase in excitation intensity, where *e-ph* coupling decay time constant reaches 3.1 ps (515 nm) and 5 ps (705 nm) under excitation with the intensity of ~90 μJ/cm^2 (Fig. 4 b). Apparently, a longer *e-ph* coupling time constant at 705 nm compared to 515 nm relates to much higher longitudinal dimension 73 nm (longitudinal mode) compared to 28 nm (transversal mode). The dimensions of nanoparticles become relevant for the *e-ph* coupling time constant under high-intensity excitation.

From Fig. 4 b, one can see that above the threshold (~12 μJ/cm^2 for trace 515 nm (Fig. 4 b) and ~5.6 μJ/cm^2 for trace 705 nm (Fig. 4 b) *e-ph* coupling (τ_1) has a linear dependence versus excitation intensity. Any *ph-ph* scattering (τ_2) dependence is unclear (Table S2), and most likely it is not dependent on the excitation intensity. Nevertheless, we observed a large increase of relative amplitude A_2 under excitation with the largest intensity (~90 μJ/cm^2) laser impulses for both traces at 515 and 705 nm (Table S2).

It is also worth mentioning that the trace at 705 nm has the largest TAS signal amplitude and possesses expressed optomechanical oscillations (presented in the next section 3.3). That could be related to the high monodispersity as the length deviation is below 16% (see Table 1).

The obtained threshold of *e-ph* coupling time constant dependence on the excitation power is quite low (~5.6 μJ/cm^2 at TAS trace of 705 nm and 12 μJ/cm^2 at TAS trace of 515 nm) in comparison to the results reported in [49] where ~50 μJ/cm^2 value for ~6.6 nm diameter Cu NPs were obtained. When the average number of photons that excite nanoparticles exceeds 1, the *e-ph* coupling time starts to depend on the excitation power linearly [28]. This could mean that the excitation pulses with intensity above 5.6 μJ/cm^2 have excited all nanorods in the analyzed sample volume at least once.

Keeping this in mind, we could assume that the low excitation energy threshold for the *e-ph* coupling time constant dependence on excitation power is most likely due to the large longitudinal dimension of Au nanorods (Fig. S1, S2, Table 1) that is represented by a 705 nm TAS trace [28]. Larger metal nanoparticles have smaller excitation intensity thresholds for *e-ph* coupling, leading to the linear dependence of *e-ph* coupling on excitation [28]. This observation could also explain why the excitation intensity threshold is larger for the 515 nm trace (LSPR transversal mode) because of the smaller transversal nanorod dimension (previously mentioned) compared to the longitudinal dimension. All in all, the analysis of the excitation intensity threshold for *e-ph* coupling time linear dependence on excitation intensity has shown that this threshold is related to the asymmetry or, in other words, differences in the transversal and longitudinal dimensions of the analyzed Au nanorods. This insight can be used for shape and size analysis of Au NPs based on *e-ph* coupling time constants calculated from TAS traces measured under large excitation intensities that exceed the mentioned threshold.

3.3. Optomechanical oscillations

During the LSPR relaxation process of phonon-phonon (*ph-ph*) scattering that follows previously discussed *e-ph* coupling, another phenomenon known as optomechanical oscillations appears

Optics EXPRESS

and it is expected in the time frames > 1 ps in parallel with the process of *ph-ph* scattering (Fig. 1 a, c) [6]. They are only visible in TAS traces of nanoparticle assemblies with low dispersion of sizes [22]. In other cases, single nanoparticles should be measured [6]. In this work, these oscillations were observed for TAS traces corresponding to a longitudinal dipole LSPR mode of Au nanorods (Fig. 5 a) and dipole LSPR of high-quality nanospheres (Fig. 5 b). That correlates with the smallest size deviations of these samples, as displayed in Table 1.

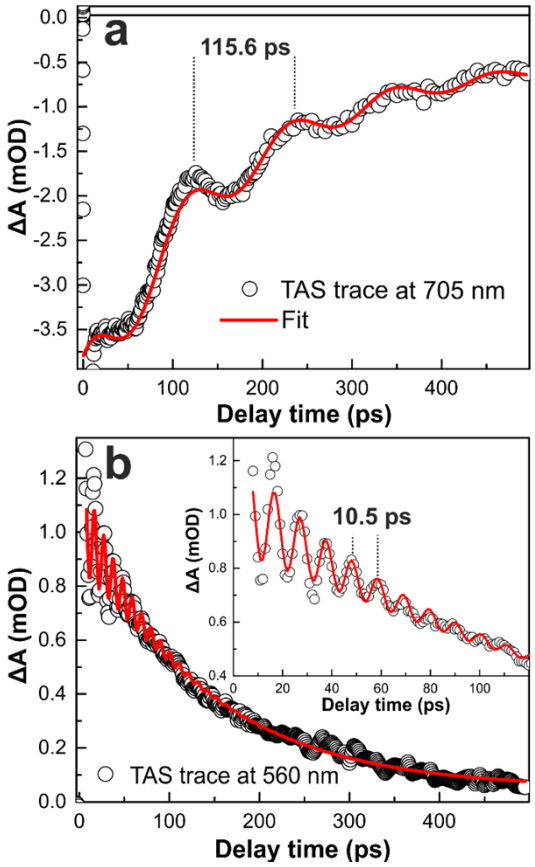

Fig. 5. The experimental TAS trace at 705 nm of Au nanorods (excited at 48 μJ/cm^2, 720 nm) (**a**) and TAS trace at 560 nm of Au high-quality nanospheres (excited at 25.6 μJ/cm^2, 350 nm) (**b**) of their fits using eq. (S2). The *e-ph* coupling trace of Au nanorods (first 20 ps) was not correctly scaled in the figure to highlight the oscillations. The inset discloses frequent oscillations in small diameter spheres that are not seen well in the same time scale as longer nanorods.

Having a closer look at the TAS trace of nanorods (Fig. 5 a) probed at 705 nm and excited at 720 nm one can see that it not only decays exponentially but also contains extra modulation that was attributed to optomechanical oscillations.

The oscillations were fitted by the damped harmonic oscillator function (eq. S2) as described in [22,32,50,51]. Based on the fitting results summarized in Table S6, we have identified optomechanical oscillations related to the longitudinal elongation of nanorods (see Fig. 1 c). In the case of highly monodisperse or single Au nanorods TAS [52], one could expect to get additional faster TAS signal trace modulation that would also indicate mechanical oscillations in the transversal direction [52]. Similar period optomechanical oscillations were registered for

Optics EXPRESS

high-quality Au nanospheres (Fig. 5 b) of a diameter very close to one of the nanorods. In that case the clearest oscillations were registered at TAS trace of 560 nm under excitation at 350 nm.

The analysis of Fig. 5 a revealed an oscillation period $T = 115.6$ ps and the damping time τ=221.1 ps (Table S6). Based on this data, we have calculated that the quality factor $Q=\pi\tau/T$ [22] is equal to 6. The rest of the fitting parameters are summarized in Table S6. The calculated oscillation period of the Au nanorods is much longer in comparison to our studied similar dimensions Au nanobipyramids (length 100 ± 1 nm) [50]. In that case oscillation period was 53.5 ps [50]. On the other hand, the oscillation period depends linearly on the size of nanoparticles [6], but it also depends on the crystalline structure, aspect ratio, and probably geometrical factor of the Au NRs, limiting the comparison of oscillation periods between Au nanorods and Au nano-bipyramid systems [6]. Based on TEM images analysis (Fig. S1), the length of Au nanorods is 74 nm, and the width of 26 nm (Table 1).

The high-quality nanospheres had optomechanical oscillations with a period of 10.5 ps, damping time of 43.5 ps, and Q factor of 13 (Table S6). As one can see, their period is smaller as expected from the differences in the dimensions. There were no optomechanical oscillations observed for Au decahedra and Au spheres with traces of nanorods. Most likely it could be attributed to the larger inhomogeneity in sizes and shapes of Au spheres with traces of nanorods while for decahedra it could be due to the incoherent boundaries between the 5-crystals (Table 1). These observations have demonstrated that optomechanical oscillation can provide extra information on the size and shape distribution of Au nanoparticles.

Comparing results obtained from the TAS and TEM measurements, it should be pointed out that during the TAS measurements, we have analyzed a much larger amount of the Au nanoparticles (the rough number was calculated based on the excitation intensity threshold (Fig. 4 b)) (in TAS $\sim 10^{11}$ versus 71 in the case of nanorods used for microscopy analysis); therefore, TAS could be treated as more reliable for the average size evaluation. In principle, the TAS results could be used to precisely evaluate the average length of Au nanorods by knowing the oscillation period [6]. Unfortunately, it is not a trivial calculation because the oscillation period also depends on the temperature, composition, and crystalline structure of the metal that should be taken into account [6].

4. Conclusions

We examined gold NPs with different shapes and monodispersity using transient absorption spectroscopy to highlight some of the advantages of dynamical optical measurements in characterizing ensembles of nanoparticles that would be obscured in steady-state optical measurements and difficult to collect in electron microscopy. The samples of monodisperse gold nanorods, high-quality nanospheres, decahedra, and nanospheres with traces of nanorods were excited with the ultrashort laser pulses with wavelengths correlating with the positions of their LSPR absorption band. The preliminary TAS spectral analysis under single excitation intensity and few time delays revealed differences in similar shape or monodispersity Au colloids that were hindered in the steady-state optical absorption spectra. Namely, TAS revealed an extra negative peak characteristic longitudinal LSPR for Au NPs with traces of nanorods and a double peak in the characteristic dipole resonance of the decahedra that was not seen in the TAS spectra of high-quality spherical NPs. The steady-state absorption appeared as a single dipolar LSPR peak of different widths in all three cases. Measurement of single TAS spectra is comparable with steady-state absorption spectra measurements by means of time.

It was shown that above the excitation intensity threshold (6 $\mu J/cm^2$ for Au NRs) there are differences between different LSPR mode (transversal or longitudinal) excited-state relaxation decay (*e-ph*) time constants but at the same time, it should be admitted that such analysis requires more measurements and is less attractive for fast shape evaluation. Another relatively quick observation is optomechanical oscillations of TAS signals that were detected in Au nanorods

Optics EXPRESS

and high-quality nanospheres. For Au nanorod colloid they were seen only under excitation of 720 nm, which we attribute to the 115.6 ps period longitudinal optomechanical vibrations. For high-quality Au nanospheres optomechanical oscillations of 10.5 ps period were observed under excitation at 350 nm, proving that they are highly monodisperse in size and shape, in agreement with TEM results. The period of optomechanical oscillations could give meaningful information about the sizes of Au nanorods or nanospheres if the crystal structure of nanoparticles is known. This information could be even more reliable than TEM image analysis because in the case of TAS the number of analyzed nanoparticles is easily 9 orders of magnitude larger. This study has shown that TAS represents a powerful and fast tool for the shape analysis and control of Au nanoparticles. We suggest that after proper calibration, TAS can be used as an efficient alternative route for Au nanoparticle shape analysis.

Funding. Lietuvos Mokslo Taryba (P-LZ-21-1); Campus France (46452XG).

Acknowledgments. Funding from the Research Council of Lithuania, Agreement No. P-LZ-21-1 is appreciated. Funding from the Région Grand Est MIPPI4D and MICA Carnot Institut and Campus France through PHC Gilibert N°46452XG.

Disclosures. The authors declare no conflicts of interest.

Data availability. Data underlying the results presented in this paper are not publicly available at this time but may be obtained from the authors upon reasonable request.

Supplemental document. See Supplement 1 for supporting content.

References

1. H. A. Atwater and A. Polman, "Plasmonics for improved photovoltaic devices," Nat. Mater. **9**(3), 205–213 (2010).
2. X. Zhang, Y. L. Chen, R. S. Liu, and D. P. Tsai, "Plasmonic photocatalysis," Rep. Prog. Phys. **76**(4), 046401 (2013).
3. C. Kuppe, K. R. Rusimova, L. Ohnoutek, D. Slavov, and V. K. Valev, ""Hot" in Plasmonics: Temperature-Related Concepts and Applications of Metal Nanostructures," Adv. Opt. Mater. **8**(1), 1901166 (2020).
4. S. S. Verma, "Plasmonics in Nanomedicine : A Review," Glob. J. Nanomed. **4**(5), 4–6 (2018).
5. Y. Gao, J. Wang, W. Wang, T. Zhao, Y. Cui, P. Liu, S. Xu, and X. Luo, "More Symmetrical "hot Spots" Ensure Stronger Plasmon-Enhanced Fluorescence: From Au Nanorods to Nanostars," Anal. Chem. **93**(4), 2480–2489 (2021).
6. G. V. Hartland, "Optical Studies of Dynamics in Noble Metal Nanostructures," Chem. Rev. **111**(6), 3858–3887 (2011).
7. "Gold Nanoparticles: Properties and Applications," https://www.sigmaaldrich.com/LT/en/technical-documents/technical-article/materials-science-and-engineering/biosensors-and-imaging/gold-nanoparticles.
8. H. Bin Jeon, P. V. Tsalu, and J. W. Ha, "Shape Effect on the Refractive Index Sensitivity at Localized Surface Plasmon Resonance Inflection Points of Single Gold Nanocubes with Vertices," Sci. Rep. **9**(1), 13635 (2019).
9. X. Huang, P. K. Jain, I. H. El-Sayed, and M. A. El-Sayed, "Gold nanoparticles: Interesting optical properties and recent applications in cancer diagnostics and therapy," Nanomedicine **2**(5), 681–693 (2007).
10. X. Huang and M. A. El-Sayed, "Plasmonic photo-thermal therapy (PPTT)," Alexandria J. Med. **47**(1), 1–9 (2011).
11. J. Hu, F. Rivero, R. A. Torres, H. Loro Ramírez, E. M. Rodríguez, F. Alfonso, J. García Solé, and D. Jaque, "Dynamic single gold nanoparticle visualization by clinical intracoronary optical coherence tomography," J. Biophotonics **10**(5), 674–682 (2017).
12. A. Dzimitrowicz, P. Jamróz, G. C. DiCenzo, I. Sergiel, T. Kozlecki, and P. Pohl, "Preparation and characterization of gold nanoparticles prepared with aqueous extracts of Lamiaceae plants and the effect of follow-up treatment with atmospheric pressure glow microdischarge," Arab. J. Chem. **12**(8), 4118–4130 (2019).
13. C. B. Murray, C. R. Kagan, and M. G. Bawendi, "Synthesis and characterization of monodispersed nanocrystals and close-packed nanocrystal assemblies," Annu. Rev. Mater. Sci. **30**(1), 545–610 (2000).
14. M. Mioc, I. Z. Pavel, R. Ghiulai, D. E. Coricovac, C. Farcaş, C.-V. Mihali, C. Oprean, V. Serafim, R. A. Popovici, C. A. Dehelean, M. I. Shtilman, A. M. Tsatsakis, and C. Şoica, "The Cytotoxic Effects of Betulin-Conjugated Gold Nanoparticles as Stable Formulations in Normal and Melanoma Cells," Front. Pharmacol. **9**, 1–16 (2018).
15. V. Amendola and M. Meneghetti, "Size evaluation of gold nanoparticles by UV-vis spectroscopy," J. Phys. Chem. C **113**(11), 4277–4285 (2009).
16. S. Ali, Y. Khan, Y. Iqbal, K. Hayat, and M. Ali, "Size determination of gold nanoparticles in silicate glasses by UV–Vis spectroscopy," J. Nanophotonics **11**(1), 016011 (2017).
17. N. De Jonge and F. M. Ross, "Electron microscopy of specimens in liquid," Nat. Nanotechnol. **6**(11), 695–704 (2011).
18. L. Wu, A. P. Fournier, J. J. Willis, M. Cargnello, and C. J. Tassone, "In Situ X-ray Scattering Guides the Synthesis of Uniform PtSn Nanocrystals," Nano Lett. **18**(6), 4053–4057 (2018).
19. D. M. Pashkov, A. A. Guda, M. V. Kirichkov, S. A. Guda, A. Martini, S. A. Soldatov, and A. V. Soldatov, "Quantitative Analysis of the UV-Vis Spectra for Gold Nanoparticles Powered by Supervised Machine Learning," J. Phys. Chem. C **125**(16), 8656–8666 (2021).

Optics EXPRESS

20. M. Maciulevičius, A. Vinčiūnas, M. Brikas, A. Butsen, N. Tarasenka, N. Tarasenko, and G. Račiukaitis, "On-Line Characterization of Gold Nanoparticles Generated by Laser Ablation in Liquids," Phys. Procedia **41**, 531–538 (2013).
21. S. Kumar and A. K. Sood, "Ultrafast Response of Plasmonic Nanostructures," in *Reviews in Plasmonics* 2015, C. D. Geddes, ed. (Springer, 2016), pp. 131–167.
22. D. Peckus, H. Rong, L. Stankevičius, M. Juodenas, S. Tamulevičius, T. Tamulevičius, and J. Henzie, "Hot Electron Emission Can Lead to Damping of Optomechanical Modes in Core-Shell Ag@TiO2 Nanocubes," J. Phys. Chem. C **121**(43), 24159–24167 (2017).
23. A. Y. Bykov, D. J. Roth, G. Sartorello, J. U. Salmón-Gamboa, and A. V. Zayats, "Dynamics of hot carriers in plasmonic heterostructures," Nanophotonics **10**(11), 2929–2938 (2021).
24. W. Huang, W. Qian, M. A. El-Sayed, Y. Ding, and Z. L. Wang, "Effect of the Lattice Crystallinity on the Electron−Phonon Relaxation Rates in Gold Nanoparticles," J. Phys. Chem. C **111**(29), 10751–10757 (2007).
25. S. Link and M. A. El-Sayed, "Shape and size dependence of radiative, non-radiative and photothermal properties of gold nanocrystals," Int. Rev. Phys. Chem. **19**(3), 409–453 (2000).
26. S. Link, C. Burda, M. Mohamed, B. Nikoobakht, and M. El-Sayed, "Femtosecond transient-absorption dynamics of colloidal gold nanorods: Shape independence of the electron-phonon relaxation time," Phys. Rev. B **61**(9), 6086–6090 (2000).
27. Y. U. Staechelin, D. Hoeing, F. Schulz, and H. Lange, "Size-Dependent Electron-Phonon Coupling in Monocrystalline Gold Nanoparticles," ACS Photonics **8**(3), 752–757 (2021).
28. J.-Y. Bigot, V. Halté, J.-C. Merle, and A. Daunois, "Electron dynamics in metallic nanoparticles," Chem. Phys. **251**(1-3), 181–203 (2000).
29. M. Pelton, J. E. Sader, J. Burgin, M. Liu, P. Guyot-Sionnest, and D. Gosztola, "Damping of Acoustic Vibrations in Gold Nanoparticles," Nat. Nanotechnol. **4**(8), 492–495 (2009).
30. M. F. Cardinal, D. Mongin, A. Crut, P. Maioli, B. Rodríguez-González, J. Pérez-Juste, L. M. Liz-Marzán, N. Del Fatti, and F. Vallée, "Acoustic Vibrations in Bimetallic Au@Pd Core–Shell Nanorods," J. Phys. Chem. Lett. **3**(5), 613–619 (2012).
31. G. Soavi, I. Tempra, M. F. Pantano, A. Cattoni, S. Collin, P. Biagioni, N. M. Pugno, and G. Cerullo, "Ultrasensitive Characterization of Mechanical Oscillations and Plasmon Energy Shift in Gold Nanorods," ACS Nano **10**(2), 2251–2258 (2016).
32. M. Juodėnas, D. Peckus, T. Tamulevičius, Y. Yamauchi, S. Tamulevičius, and J. Henzie, "Effect of Ag Nanocube Optomechanical Modes on Plasmonic Surface Lattice Resonances," ACS Photonics **7**(11), 3130–3140 (2020).
33. G. Kedawat, I. Sharma, K. Nagpal, M. Kumar, G. Gupta, and B. K. Gupta, "Studies of ultrafast transient absorption spectroscopy of gold nanorods in an aqueous solution," ACS Omega **4**(7), 12626–12631 (2019).
34. K. N. Krishnakanth, B. Chandu, M. S. S. Bharathi, S. S. Kumar Raavi, and S. V. Rao, "Ultrafast excited state dynamics and femtosecond nonlinear optical properties of laser fabricated Au and Ag50Au50 nanoparticles," Optical Materials **95**, 109239 (2019).
35. G. V. Hartland, M. Hu, O. Wilson, P. Mulvaney, and John E. Sader, "Coherent Excitation of Vibrational Modes in Gold Nanorods G," J. Phys. Chem. B **106**(4), 743–747 (2002).
36. J. Wu, D. Xiang, and R. Gordon, "Characterizing gold nanorods in aqueous solution by acoustic vibrations probed with four-wave mixing," Opt. Express **24**(12), 12458 (2016).
37. R. J. Newhouse, H. Wang, J. K. Hensel, D. A. Wheeler, S. Zou, and J. Z. Zhang, "Coherent vibrational oscillations of hollow gold nanospheres," J. Phys. Chem. Lett. **2**(3), 228–235 (2011).
38. N. G. Bastús, J. Comenge, and V. Puntes, "Kinetically controlled seeded growth synthesis of citrate-stabilized gold nanoparticles of up to 200 nm: Size focusing versus ostwald ripening," Langmuir **27**(17), 11098–11105 (2011).
39. Q. Li, F. Wang, Y. Bai, L. Xu, Y. Yang, L. Yan, S. Hu, B. Zhang, S. Dai, and Z. Tan, "Decahedral-shaped Au nanoparticles as plasmonic centers for high performance polymer solar cells," Org. Electron. **43**, 33–40 (2017).
40. J. Cao, T. Sun, and K. T. V. Grattan, "Gold nanorod-based localized surface plasmon resonance biosensors: A review," Sens. Actuators, B **195**, 332–351 (2014).
41. V. Myroshnychenko, J. Rodríguez-Fernández, I. Pastoriza-Santos, A. M. Funston, C. Novo, P. Mulvaney, L. M. Liz-Marzán, F. j, and García de Abajo, "Modelling the optical response of gold nanoparticles," Chem. Soc. Rev. **37**(9), 1792 (2008).
42. M.-N. Su, C. J. Ciccarino, S. Kumar, P. D. Dongare, S. A. Hosseini Jebeli, D. Renard, Y. Zhang, B. Ostovar, W.-S. Chang, P. Nordlander, N. J. Halas, R. Sundararaman, P. Narang, and S. Link, "Ultrafast Electron Dynamics in Single Aluminum Nanostructures," Nano Lett. **19**(5), 3091–3097 (2019).
43. X. Zhang, C. Huang, M. Wang, P. Huang, X. He, and Z. Wei, "Transient localized surface plasmon induced by femtosecond interband excitation in gold nanoparticles," Sci. Rep. **8**(1), 10499 (2018).
44. M. Priyadarshini, M. Adnan, and G. V. Prakash, "Linear and nonlinear excitation induced ultrafast absorption dynamics in laser ablated and chemically synthesized gold nanoparticle colloids," Opt. Mater. **117**, 111206 (2021).
45. A. Iagatti, B. Shao, A. Credi, B. Ventura, I. Aprahamian, and M. Di Donato, "Ultrafast processes triggered by one- and two-photon excitation of a photochromic and luminescent hydrazone," Beilstein J. Org. Chem. **15**, 2438–2446 (2019).
46. D. Peckus, Š. Meškinis, A. Vasiliauskas, E. Rajackaitė, M. Andrulevičius, V. Kopustinskas, and S. Tamulevičius, "Structure and optical properties of diamond like carbon films containing aluminium and alumina," Appl. Surf. Sci. **529**, 147040 (2020).

Optics EXPRESS

47. A. Sánchez-Iglesias, N. Winckelmans, T. Altantzis, S. Bals, M. Grzelczak, and L. M. Liz-Marzán, "High-Yield Seeded Growth of Monodisperse Pentatwinned Gold Nanoparticles through Thermally Induced Seed Twinning," J. Am. Chem. Soc. **139**(1), 107–110 (2017).
48. E. Carbó-Argibay and B. Rodríguez-González, "Controlled Growth of Colloidal Gold Nanoparticles: Single-Crystalline versus Multiply-twinned Particles," Isr. J. Chem. **56**(4), 214–226 (2016).
49. D. Peckus, T. Tamulevičius, Š. Meškinis, A. Tamulevičienė, A. Vasiliauskas, O. Ulčinas, V. Gulbinas, and S. Tamulevičius, "Linear and Nonlinear Absorption Properties of Diamond-Like Carbon Doped With Cu Nanoparticles," Plasmonics **12**(1), 47–58 (2017).
50. D. Peckus, J. Henzie, T. Tamulevičius, M. Andrulevičius, A. Lazauskas, E. Rajackaitė, Š. Meškinis, and S. Tamulevičius, "Ultrafast relaxation dynamics of aluminum nanoparticles in solution," Phys. E (Amsterdam, Neth.) **117**, 113795 (2020).
51. S. Chen, R. Niu, W. Wu, D. Kong, and Y. Gao, "Wavelength-dependent nonlinear absorption and ultrafast dynamics process of Au triangular nanoprisms," Opt. Express **27**(13), 18146 (2019).
52. P. Zijlstra, A. L. Tchebotareva, J. W. M. Chon, M. Gu, and M. Orrit, "Acoustic Oscillations and Elastic Moduli of Single Gold Nanorods," Nano Lett. **8**(10), 3493–3497 (2008).